On the Closed-Form Detection Error Rate Analysis in Physical Layer Anonymous Communications

Yifan Cui, *Student Member, IEEE*, Zhongxiang Wei, *Member, IEEE*, Christos Masouros, *Senior Member, IEEE*, Xu Zhu, *Senior Member, IEEE*, and Hong Tang

***Abstract*—In recent years, physical layer (PHY) anonymous precoding has become imperative in applications that carry personal and sensitive data. While manipulating the signaling pattern of transmitted signals for obtaining high communication utility, the anonymous precoding masks the sender's PHY characteristics for the purpose of sender anonymity. Nevertheless, the anonymity provided by anonymous precoding has only been numerically demonstrated, and the relevant literature still lacks analytic results regarding the detection error rate (DER) performance. In this paper, we give the first attempt to show an analytic DER result of generic precoders. Tight closed-form DER expression is derived, as a function of the precoder employed at the sender, block length, propagation channel, and noise status. Some important properties are revealed, such as the impacts of block length, noise, and channel correlation on the DER result. Finally, simulation results validate that the normalized mean squared error (NMSE) between the closed-form and actual DER results is on the levels of $0 \sim 10^{-1}$. The proposed analytic DER results help easily quantify the anonymity performance of existing anonymity-agnostic and anonymous precoders.**

***Index Terms*—Closed-form DER, anonymous communications, physical layer, anonymous precoding.**

I. Introduction

In the era of the Internet of Things, provision of security and privacy is a pervasive issue. In general, the purpose of data security is to prevent confidential communication from being exploited or attacked by external eavesdroppers. Authentication [1], cryptography [2], covert communication [3], securing beamforming and other methods [4] from the PHY to the upper layers of networks have been extensively studied for security. By contrast, the aim of privacy protection is to minimize the receiver's capability to infer the non-shared information, while guaranteeing the communication quality of the same receiver for utility [5]. For example, when receiving signal for utility in smart homes and telemedicine, a legitimate but curious receiver may infer the user's non-shared data, such as users' identity/age/health metrics, lifestyle and whereabouts. Hence, when communicating with service providers for utility, users wish to remain anonymous towards the receiver for avoiding potential cyberfraud, known as anonymous communications.

On the upper layers of networks, a bundle of anonymous protection strategies have been studied, including anonymous encryption [6], anonymous authentication [7], routing designs [8] and so on. These techniques conceal users' characteristics of the higher layers, such as their identities (ID)s or media access control/Internet protocol addresses. As a further step, the work in [5] points out that the signaling pattern at the PHY can also be leveraged to unmask sender information. To be specific, when employing classic minimum mean squared error (MMSE), zero-forcing (ZF) [9], singular value decomposition (SVD) [10], power minimization (PM) [11] and other anonymity-agnostic precoders, the pattern of the received signal is coupled with the user's unique channel state information (CSI). As the differences among users' channels commonly exist in wireless communications, CSIs can be regarded as the PHY IDs of the users. Therefore, the receiver is able to identify the sender by extracting the correct CSI from the received signal. Since the sender detection can be realized only with the PHY information, it invalidates the anonymous protection schemes on the upper layers of networks. As a countermeasure at the PHY, anonymous precoding [5] is capable of concealing a sender's CSI from the transmitted signal, thereby scrambling the accuracy of sender detection at the receiver side [5].

Nevertheless, the provision of anonymity by the anonymous precoder has only been numerically evaluated. The work in [5] was the first to show that, with an empirical anonymous constraint, the pattern of the transmitted signal can be controlled for the purpose of sender anonymity. The design in [12] pointed out that a stricter value of anonymous constraint is able to better guarantee the anonymity, thus deteriorating the DER performance of the receiver. Despite of recent progress made, the analytic DER performance achieved by different precoders is still an open challenge. As a result, the anonymity performance gain of the anonymous precoder

Yifan Cui and Zhongxiang Wei are with the College of Electronic and Information Engineering, Tongji University, Shanghai 200092, China (e-mail: 2230692, z_wei@tongji.edu.cn). Corresponding author: Zhongxiang Wei.

Christos Masouros is with the Department of Electronic and Electrical Engineering, University College London, London WC1E 6BT, U.K. (e-mail: c.masouros@ucl.ac.uk).

Xu Zhu is with the School of Electronic and Information Engineering, Harbin Institute of Technology, Shenzhen 518055, China (e-mail: xuzhu@stu.hit.edu.cn).

Hong Tang is with the School of Electronic and Information Engineering, Chongqing University of Posts and Telecommunication, Chongqing 400065, China (e-mail: tangh@cqupt.edu.cn).

This work was supported in part by the Natural Science Foundation of China (NSFC) under Grant 62101384/62171161, in part by the Guangdong Basic and Applied Basic Research Foundation under Grants 2021A1515011832/2022B1515120018, in part by the Shenzhen Key Laboratory under Grant ZDSYS20210623091808025, in part by the Shenzhen Science and Technology Program under Grant KQTD20190929172545139, in part by the Chongqing Key Laboratory of Mobile Communication Technology under Grant cqupt-mct-202101, and in part by the open research fund of National Mobile Communications Research Laboratory under Grant 2024D08.

has not been quantified yet. This further hinders researcher from flexibly balancing the anonymity and communication performance. Motivated by this issue, in this paper, we attempt to present theoretical analysis of the DER performance. Our contributions are summarized as follows.

Exploiting the statistics of the signal, we first demonstrate the analytic DER performance of two classic PHY sender detectors, i.e., the maximum Frobenius norm (MFN) and the maximum likelihood estimation (MLE) detectors. The tight closed-form expression of DER is derived, as a function of the precoder employed at the sender, block length, propagation channel, and noise status. Then, we evaluate the DER of several classic anonymity-agnostic precoders, as well as anonymous precoders. Also, a series of important properties regarding the PHY anonymity have been revealed.

Notation: Matrices and vectors are represented by boldface capital and lower case letters, respectively. $\boldsymbol{I}_n$ denotes an n-by-n identity matrix. $[\boldsymbol{A}]_{mn}$ abstracts the element in row m and column n of a matrix. $\boldsymbol{A}^H$, $\mathrm{tr}(\boldsymbol{A})$ and $\|\boldsymbol{A}\|_F$ denote the Hermitian transpose, trace and Frobenius norm of a matrix. $\|\boldsymbol{x}\|_2$ denotes the 2-norm of a vector. $|\cdot|$ denotes absolute value of a complex number. $\mathcal{N}\{\cdot\}$ and $\mathcal{CN}\{\cdot\}$ represent Gaussian distribution and complex Gaussian distribution. $\Pr(a|b)$ denotes the conditional probability of a given b. $\mathbb{E}\{\cdot\}$ and $\mathbb{V}\{\cdot\}$ denote expectation and variance of a random variable. $\mathrm{cov}\{a,b\}$ denotes covariance of two random variables.

II. System Model and Sender Detection Strategies

In this section, system model and PHY sender detectors are introduced in subsections II-A and II-B.

A. System Model

Consider an uplink multiuser multiple-input and multiple-output (MIMO) transmission scenario, where a group of users $\mathbb{K}$ ($|\mathbb{K}| = K$) send signals to a base station (BS) under time-division-multiple-access. In particular, users remain anonymous during the transmission phase. That is, the BS can correctly receive the data but cannot identify which user is the real sender. Assume that each user is equipped with N_t transmit-antennas, while the BS is equipped with N_r receive-antennas. Define $\boldsymbol{H}_k \in \mathbb{C}^{N_r \times N_t}$ as the block-fading MIMO channel between the k-th user and the BS. As the sender detection is performed at the block level, denote L as block length. Define $\boldsymbol{W}_k \in \mathbb{C}^{N_t \times N_s}$ as the precoding matrix of the k-th user, and $\boldsymbol{S}_k \in \mathbb{C}^{N_s \times L}$ as the symbol matrix transmitted by the k-th user, where N_s denotes the number of symbols transmitted per slot depending on the specific multiplexing strategy. Denote $\boldsymbol{N} \in \mathbb{C}^{N_r \times L}$ as the circularly symmetric complex Gaussian noise with noise variance σ^2 and element as $[\boldsymbol{N}]_{mn} \sim \mathcal{CN}(0, \sigma^2)$. Without loss of generality, assume that the k-th user sends signal to the BS in the considered block, and the received signal at the BS is written as

$$\boldsymbol{Y} = \boldsymbol{H}_k \boldsymbol{W}_k \boldsymbol{S}_k + \boldsymbol{N}. \tag{1}$$

At the PHY, the BS only analyzes the received signal and the inherent characteristics of the wireless channels to detect the sender. The sender detection can be formulated as a multiple hypotheses testing (MHT) problem [5]

$$\boldsymbol{Y} = \begin{cases} \mathcal{H}_0 : \boldsymbol{N}, \\ \mathcal{H}_1 : \boldsymbol{H}_1 \boldsymbol{W}_1 \boldsymbol{S}_1 + \boldsymbol{N}, \\ \quad \vdots \\ \mathcal{H}_K : \boldsymbol{H}_K \boldsymbol{W}_K \boldsymbol{S}_K + \boldsymbol{N}, \end{cases} \tag{2}$$

where the hypothesis $\mathcal{H}_0$ denotes that only noise appears at the BS, while hypothesis $\mathcal{H}_k$ means a signal coming from the k-th user is received.

B. Sender Detection Strategies

In this subsection, the MFN and the MLE sender detectors are briefly discussed for the sake of completeness, while the details can be found in [5]. For handling the MHT problem in (2), the BS can first detect the presence of a signal, generally solved by the classic energy detection [13]. The test statistic is given by $\mathit{\Gamma}(\boldsymbol{Y}) = \frac{\|\boldsymbol{Y}\|_F^2}{LN_r}$. On comparing $\mathit{\Gamma}(\boldsymbol{Y})$ against a detection threshold ε, the hypothesis $\mathcal{H}_0$ is determined to be true when $\mathit{\Gamma}(\boldsymbol{Y}) < \varepsilon$, and to be false otherwise. Once $\mathcal{H}_0$ is decided to be a false hypothesis, i.e., the BS confirming the presence of an incoming signal, it turns to detect the sender of the signal (hypothesis $\mathcal{H}_1$ to $\mathcal{H}_K$). Since the propagation channel can be regarded as the unique PHY identity of the user, the detection is essentially the identification of the channel from which the signal is actually transmitted.

1) MFN Sender Detection: The philosophy of the MFN detection is to leverage the match filter for sender detection. First, the received signal is equalized with different $\boldsymbol{H}_i^H, \forall i \in \mathbb{K}$. Since $\|\boldsymbol{H}_k^H \boldsymbol{H}_k\|_F^2$ is more likely to be larger than $\|\boldsymbol{H}_i^H \boldsymbol{H}_k\|_F^2$, $\forall i \neq k, i \in \mathbb{K}$, the resulted F-norm $G_k = \|\boldsymbol{H}_k^H \boldsymbol{Y}\|_F^2 = \|\boldsymbol{H}_k^H \boldsymbol{H}_k \boldsymbol{W}_k \boldsymbol{S}_k + \boldsymbol{H}_k^H \boldsymbol{N}\|_F^2$ calculated by the correct hypothesis channel $\boldsymbol{H}_k$ has a high probability to be higher than the norm $G_i = \|\boldsymbol{H}_i^H \boldsymbol{Y}\|_F^2 = \|\boldsymbol{H}_i^H \boldsymbol{H}_k \boldsymbol{W}_k \boldsymbol{S}_k + \boldsymbol{H}_i^H \boldsymbol{N}\|_F^2$, calculated by a false hypothesis channel $\boldsymbol{H}_i$. Thus, the MFN sender detection is written as $\Psi_{\mathrm{MFN}} = \arg\max\limits_{k \in \mathbb{K}} \{\|\boldsymbol{H}_1^H \boldsymbol{Y}\|_F^2, \ldots, \|\boldsymbol{H}_K^H \boldsymbol{Y}\|_F^2\}$. The MFN detector can be used for arbitrary number of N_t ($N_t > 1$).

2) MLE Sender Detection: The philosophy of the MLE detection is to estimate the transmitted signal with different users' channels, and then compute the Euclidean distance between the reconstructed and actual received signals. Explicitly, if the i-th ($i \neq k$) user's channel is exploited for estimation, a reconstructed signal is given as $\hat{\boldsymbol{Y}}_i = \boldsymbol{H}_i \boldsymbol{H}_i^\dagger \boldsymbol{Y} = \boldsymbol{H}_i \boldsymbol{H}_i^\dagger \boldsymbol{H}_k \boldsymbol{W}_k \boldsymbol{S}_k + \boldsymbol{H}_i \boldsymbol{H}_i^\dagger \boldsymbol{N}$, where $\boldsymbol{H}_i^\dagger = (\boldsymbol{H}_i^H \boldsymbol{H}_i)^{-1} \boldsymbol{H}_i^H$. Then, the Euclidean distance between the reconstructed and actual received signal is calculated as $D_i = \|\boldsymbol{Y} - \hat{\boldsymbol{Y}}_i\|_F^2 = \|(\boldsymbol{H}_i \boldsymbol{H}_i^\dagger - \boldsymbol{I}_{N_r}) \boldsymbol{H}_k \boldsymbol{W}_k \boldsymbol{S}_k + (\boldsymbol{H}_i \boldsymbol{H}_i^\dagger - \boldsymbol{I}_{N_r}) \boldsymbol{N}\|_F^2$. In a similar vein, when the real sender k's channel is exploited for detection, the Euclidean distance is computed as $D_k = \|(\boldsymbol{H}_k \boldsymbol{H}_k^\dagger - \boldsymbol{I}_{N_r}) \boldsymbol{N}\|_F^2$, where $\boldsymbol{H}_k^\dagger = (\boldsymbol{H}_k^H \boldsymbol{H}_k)^{-1} \boldsymbol{H}_k^H$. As D_k only contains a noise term, there is a high probability that $D_i > D_k$. Therefore, the MLE sender detection algorithm is expressed as $\Psi_{\mathrm{MLE}} = \arg\min\limits_{k \in \mathbb{K}} \{\|(\boldsymbol{H}_1 \boldsymbol{H}_1^\dagger - \boldsymbol{I}_{N_r}) \boldsymbol{Y}\|_F^2, \ldots, \|(\boldsymbol{H}_K \boldsymbol{H}_K^\dagger - \boldsymbol{I}_{N_r}) \boldsymbol{Y}\|_F^2\}$. The MLE detector only works in the case of $N_r > N_t$.

It is because when $N_r \leq N_t$, the pseudo-inverse result $\boldsymbol{H}_k^{\dagger} = (\boldsymbol{H}_k^H \boldsymbol{H}_k)^{-1} \boldsymbol{H}_k^H$ becomes incomputable due to the rank-insufficient matrices $\boldsymbol{H}_k^H \boldsymbol{H}_k$.

III. Analysis of Detection Error Rate Performance

In this section, the DER performance of the MFN and MLE detectors is quantified with tight closed-form expressions.

A. DER Analysis of MFN Detector

Exploiting the MHT problem (2), evidently, DER is the probability that under $\mathcal{H}_k$, the BS falsely declaring either that no signal is received, or that a signal is transmitted from a user other than the k-th user, written as

$$\zeta_{\mathrm{MFN}} = 1 - \Pr(\mathit{\Gamma}(\boldsymbol{Y}) \geq \varepsilon | \mathcal{H}_k) \prod_{i, i \neq k}^{K} \Pr(G_i \leq G_k | \mathcal{H}_k). \tag{3}$$

The term $\Pr(\mathit{\Gamma}(\boldsymbol{Y}) \geq \varepsilon | \mathcal{H}_k)$ denotes the probability that under $\mathcal{H}_k$, the BS correctly identifies an incoming signal. The term $\prod_{i,i\neq k}^{K} \Pr(G_i \leq G_k | \mathcal{H}_k)$ denotes the probability that the BS correctly identifies user k as the sender. Assuming that the signal is transmitted through the Rayleigh channel, the test statistic $\mathit{\Gamma}(\boldsymbol{Y})$ of the energy detector follows chi-square distribution with $2N_r L$ degree of freedom and non-centrality parameter $\frac{2\|\boldsymbol{H}_k \boldsymbol{W}_k \boldsymbol{S}_k\|_F^2}{\sigma^2}$ [13]. Hence, the term $\Pr(\mathit{\Gamma}(\boldsymbol{Y}) \geq \varepsilon | \mathcal{H}_k)$ is calculated as

$$\Pr(\mathit{\Gamma}(\boldsymbol{Y}) \geq \varepsilon | \mathcal{H}_k) = 1 - \Pr(\mathit{\Gamma}(\boldsymbol{Y}) < \varepsilon | \mathcal{H}_k) = 1 - \mathcal{C}\left(\frac{2N_r \varepsilon L}{\sigma^2}\right), \tag{4}$$

where $\mathcal{C}(\cdot)$ denotes the cumulative distribution function of the non-central chi-square distributed variable $\mathit{\Gamma}(\boldsymbol{Y})$. To calculate the term $\Pr(G_i \leq G_k | \mathcal{H}_k)$, we first investigate the statistics of G_k and G_i as summarized in Lemma 1.

Lemma 1: Define $\boldsymbol{U}_i = \boldsymbol{H}_i^H \boldsymbol{H}_k \boldsymbol{W}_k \boldsymbol{S}_k$. The expectation and variance of G_i are given as

$$\mathbb{E}\{G_i\} = L\sigma^2 \mathrm{tr}(\boldsymbol{H}_i \boldsymbol{H}_i^H) + \mathrm{tr}(\boldsymbol{U}_i^H \boldsymbol{U}_i), \tag{5}$$

and

$$\mathbb{V}\{G_i\} = L\sigma^4 \mathrm{tr}(\boldsymbol{H}_i \boldsymbol{H}_i^H \boldsymbol{H}_i \boldsymbol{H}_i^H) + 2\sigma^2 \mathrm{tr}(\boldsymbol{U}_i^H \boldsymbol{H}_i^H \boldsymbol{H}_i \boldsymbol{U}_i). \tag{6}$$

Proof of Lemma 1: please see Appendix. ■

The expectation and variance of G_k can be obtained in the same manner. Although the expectation and variance of G_i are given by Lemma 1, it is still difficult to obtain an exact probability density function (pdf) of G_i. The exact pdf of such a quadratic form was presented in [14]. However, it involves complicated integral calculations, which limits its application in our DER analysis. Fortunately, as G_i in fact contains the summation of $N_r L$ samples, it can be approximated as a Gaussian distributed variable based on central limit theorem.

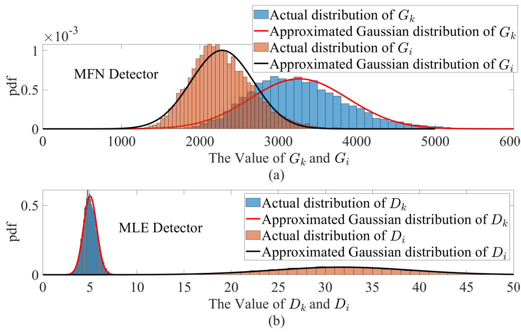

(a)

(b)

Fig. 1. The actual and approximated pdfs of the values of G_k, G_i, D_k and D_i. MMSE precoder is employed by the sender [9], signal-to-noise ratio (SNR) is set to 10 dB.

Fig. 1 (a) shows that the values of G_i and G_k indeed approximately follow Gaussian distributions. Denote $p(x)$ and $q(x)$ as two probability distributions of a discrete random variable x, the Kullback–Leibler (KL) divergence of $q(x)$ from $p(x)$ is defined as $\mathrm{D}_{\mathrm{KL}}(p(x)\|q(x)) = \sum_{x\in X} p(x) \ln \frac{p(x)}{q(x)}$. In particular, $\mathrm{D}_{\mathrm{KL}}(p(x)\|q(x)) = 0$ if and only if $p(x)$ and $q(x)$ are exactly the same distribution. Denote $\mathcal{N}_{G_k}$ as the Gaussian random variable that is used to approximate G_k, and $\mathcal{N}_{G_i}$ as the Gaussian random variable that is used to approximate G_i. With the simulation setup in Fig. 1 (a), we obtain the KL divergence $\mathrm{D}_{\mathrm{KL}}(G_k\|\mathcal{N}_{G_k}) = 0.0304$ and $\mathrm{D}_{\mathrm{KL}}(G_i\|\mathcal{N}_{G_i}) = 0.0274$, which means that the distributions of G_k and G_i can be well approximated by Gaussian distributions. More importantly, G_k and G_i show distinct expectations and variances, which thus can be used to distinguish the two statistics.

Defining $\gamma_i = G_k - G_i$, its expectation and variance are

$$\begin{aligned} \mathbb{E}\{\gamma_i\} &= \mathbb{E}\{G_k\} - \mathbb{E}\{G_i\} \\ &= L\sigma^2 \mathrm{tr}(\boldsymbol{H}_k \boldsymbol{H}_k^H - \boldsymbol{H}_i \boldsymbol{H}_i^H) + \mathrm{tr}(\boldsymbol{U}_k^H \boldsymbol{U}_k - \boldsymbol{U}_i^H \boldsymbol{U}_i), \end{aligned} \tag{7}$$

and

$$\begin{aligned} \mathbb{V}\{\gamma_i\} &= \mathbb{V}\{G_k\} + \mathbb{V}\{G_i\} + \mathrm{cov}\{G_k, G_i\} \\ &= L\sigma^4 \mathrm{tr}(\boldsymbol{H}_k \boldsymbol{H}_k^H \boldsymbol{H}_k \boldsymbol{H}_k^H + \boldsymbol{H}_i \boldsymbol{H}_i^H \boldsymbol{H}_i \boldsymbol{H}_i^H) \\ &\quad + 2\sigma^2 \mathrm{tr}(\boldsymbol{U}_k^H \boldsymbol{H}_k^H \boldsymbol{H}_k \boldsymbol{U}_k + \boldsymbol{U}_i^H \boldsymbol{H}_i^H \boldsymbol{H}_i \boldsymbol{U}_i), \end{aligned} \tag{8}$$

where the covariance term $\mathrm{cov}\{G_k, G_i\}$ is ignored because G_k and G_i are weakly correlated. Given that γ_i follows Gaussian distribution, we have

$$\begin{aligned} &\Pr(G_i \leq G_k | \mathcal{H}_k) = \Pr(\gamma_i \geq 0 | \mathcal{H}_k) \\ &= \int_0^{\infty} f_{\gamma_i}(t) \mathrm{d}t = \frac{1}{2}\left(1 + \mathrm{erf}\left(\frac{\mathbb{E}(\gamma_i)}{\sqrt{2\mathbb{V}(\gamma_i)}}\right)\right), \end{aligned} \tag{9}$$

where $f_{\gamma_i}(\cdot)$ denotes the pdf of the variable γ_i, and $\mathrm{erf}(\cdot)$ denotes the Gaussian error function. Substituting (7) and (8) into (9), $\Pr(\gamma_i \geq 0 | \mathcal{H}_k)$ is rewritten as (10). Substituting (4) and (10) into (3) leads a tight closed-form DER expression of the MFN detector in (11), as shown at the top of the page.

As the term $\mathcal{C}\left(\frac{2N_r \varepsilon L}{\sigma^2}\right)$ approaches 0 when ε is a small value, the miss detection rate can be omitted. Based on the Neyman-Pearson criterion, the probability of false alarm may be raised by the small valued ε. However, its effect can be significantly reduced on account of the multiple antennas at the receiver. Ignoring the effect of miss detection, a tight expression of DER is given as (12), which is shown at the top of the next page.

Remark 1: The value of the term $\mathrm{tr}(\boldsymbol{U}_k^H \boldsymbol{U}_k - \boldsymbol{U}_i^H \boldsymbol{U}_i)$ is typically a non-zero finite number, when anonymity-agnostic precoders are employed. As the term $\mathrm{tr}(\boldsymbol{H}_k \boldsymbol{H}_k^H - \boldsymbol{H}_i \boldsymbol{H}_i^H)$ approaches 0, a small value of noise makes the value of the error function in (12) approach 1, where the DER approaches 0. Hence, the principle of the anonymous precoder against the MFN detector is to manipulate the term $\mathrm{tr}(\boldsymbol{U}_k^H \boldsymbol{U}_k - \boldsymbol{U}_i^H \boldsymbol{U}_i)$,

$$\Pr(\gamma_i \geq 0|\mathcal{H}_k) = \frac{1}{2}\left(1+\operatorname{erf}\left(\frac{L\sigma^2\operatorname{tr}(\boldsymbol{H}_k\boldsymbol{H}_k^H-\boldsymbol{H}_i\boldsymbol{H}_i^H)+\operatorname{tr}(\boldsymbol{U}_k^H\boldsymbol{U}_k-\boldsymbol{U}_i^H\boldsymbol{U}_i)}{\sqrt{2L\sigma^4\operatorname{tr}(\boldsymbol{H}_k\boldsymbol{H}_k^H\boldsymbol{H}_k\boldsymbol{H}_k^H+\boldsymbol{H}_i\boldsymbol{H}_i^H\boldsymbol{H}_i\boldsymbol{H}_i^H)+4\sigma^2\operatorname{tr}(\boldsymbol{U}_k^H\boldsymbol{H}_k^H\boldsymbol{H}_k\boldsymbol{U}_k+\boldsymbol{U}_i^H\boldsymbol{H}_i^H\boldsymbol{H}_i\boldsymbol{U}_i)}}\right)\right). \tag{10}$$

$$\zeta_{MFN} = 1-\left(1-\mathcal{C}\left(\tfrac{2N_r\varepsilon L}{\sigma^2}\right)\right)\prod_{i,i\neq k}^{K}\frac{1}{2}\left(1+\operatorname{erf}\left(\frac{L\sigma^2\operatorname{tr}(\boldsymbol{H}_k\boldsymbol{H}_k^H-\boldsymbol{H}_i\boldsymbol{H}_i^H)+\operatorname{tr}(\boldsymbol{U}_k^H\boldsymbol{U}_k-\boldsymbol{U}_i^H\boldsymbol{U}_i)}{\sqrt{2L\sigma^4\operatorname{tr}(\boldsymbol{H}_k\boldsymbol{H}_k^H\boldsymbol{H}_k\boldsymbol{H}_k^H+\boldsymbol{H}_i\boldsymbol{H}_i^H\boldsymbol{H}_i\boldsymbol{H}_i^H)+4\sigma^2\operatorname{tr}(\boldsymbol{U}_k^H\boldsymbol{H}_k^H\boldsymbol{H}_k\boldsymbol{U}_k+\boldsymbol{U}_i^H\boldsymbol{H}_i^H\boldsymbol{H}_i\boldsymbol{U}_i)}}\right)\right). \tag{11}$$

$$\zeta_{MFN} = 1-\prod_{i,i\neq k}^{K}\frac{1}{2}\left(1+\operatorname{erf}\left(\frac{L\sigma^2\operatorname{tr}(\boldsymbol{H}_k\boldsymbol{H}_k^H-\boldsymbol{H}_i\boldsymbol{H}_i^H)+\operatorname{tr}(\boldsymbol{U}_k^H\boldsymbol{U}_k-\boldsymbol{U}_i^H\boldsymbol{U}_i)}{\sqrt{2L\sigma^4\operatorname{tr}(\boldsymbol{H}_k\boldsymbol{H}_k^H\boldsymbol{H}_k\boldsymbol{H}_k^H+\boldsymbol{H}_i\boldsymbol{H}_i^H\boldsymbol{H}_i\boldsymbol{H}_i^H)+4\sigma^2\operatorname{tr}(\boldsymbol{U}_k^H\boldsymbol{H}_k^H\boldsymbol{H}_k\boldsymbol{U}_k+\boldsymbol{U}_i^H\boldsymbol{H}_i^H\boldsymbol{H}_i\boldsymbol{U}_i)}}\right)\right). \tag{12}$$

and make it approach or even less than 0. As a result, the value of the error function in (12) approaches or is less than 0, thus scrambling the DER performance.

B. DER Analysis of MLE Detector

Recalling the MLE detection, its DER is expressed as

$$\zeta_{\mathrm{MLE}} = 1-\Pr(\mathit{\Gamma}(\boldsymbol{Y})\geq\varepsilon|\mathcal{H}_k)\prod_{i,i\neq k}^{K}\Pr(D_i\geq D_k|\mathcal{H}_k). \tag{13}$$

To calculate the term $\Pr(D_i \geq D_k|\mathcal{H}_k)$, we first investigate the distributions of D_k and D_i. For the sake of simplicity, denote $\boldsymbol{\Theta}_i = \boldsymbol{H}_i\boldsymbol{H}_i^{\dagger} - \boldsymbol{I}_{N_r}$ and $\boldsymbol{V}_i = \boldsymbol{\Theta}_i\boldsymbol{H}_k\boldsymbol{W}_k\boldsymbol{S}_k$. The expectation and variance of D_i are summarized in Lemma 2.

Lemma 2: The expectation and variance of D_i are given as

$$\mathbb{E}\{D_i\} = L\sigma^2\operatorname{tr}(\boldsymbol{\Theta}_i\boldsymbol{\Theta}_i^H) + \operatorname{tr}(\boldsymbol{V}_i^H\boldsymbol{V}_i), \tag{14}$$

and

$$\mathbb{V}\{D_i\} = L\sigma^4\operatorname{tr}(\boldsymbol{\Theta}_i\boldsymbol{\Theta}_i^H\boldsymbol{\Theta}_i\boldsymbol{\Theta}_i^H) + 2\sigma^2\boldsymbol{V}_i^H\boldsymbol{\Theta}_i^H\boldsymbol{\Theta}_i\boldsymbol{V}_i. \tag{15}$$

The proof of Lemma 2 is similar to that of Lemma 1, and thus is omitted due to page limit. ■

Similarly, the expectation and variance of D_k are given as

$$\mathbb{E}\{D_k\} = L\sigma^2\operatorname{tr}(\boldsymbol{\Theta}_k\boldsymbol{\Theta}_k^H), \tag{16}$$

and

$$\mathbb{V}\{D_k\} = L\sigma^4\operatorname{tr}(\boldsymbol{\Theta}_k\boldsymbol{\Theta}_k^H\boldsymbol{\Theta}_k\boldsymbol{\Theta}_k^H). \tag{17}$$

Again leveraging the central limit theorem, D_i and D_k approximately follow Gaussian distributions. Fig. 1 (b) demonstrates that, the approximated Gaussian variables indeed match the actual simulation results. Denote $\mathcal{N}_{D_k}$ and $\mathcal{N}_{D_i}$ as the Gaussian random variables that are used to approximate D_k and D_i, respectively. With the simulation setup in Fig. 1 (b), the terms $\mathrm{D}_{\mathrm{KL}}(D_k\|\mathcal{N}_{D_k})$ and $\mathrm{D}_{\mathrm{KL}}(D_i\|\mathcal{N}_{D_i})$ are calculated as 0.0094 and 0.0139. It indicates that the distributions of D_k and D_i also can be approximated by Gaussian distributions. Defining $\rho_i = G_k - G_i$, its expectation is

$$\begin{aligned}\mathbb{E}\{\rho_i\} &= \mathbb{E}\{D_k\} - \mathbb{E}\{D_i\}\\ &= L\sigma^2\operatorname{tr}(\boldsymbol{\Theta}_k\boldsymbol{\Theta}_k^H - \boldsymbol{\Theta}_i\boldsymbol{\Theta}_i^H) - \operatorname{tr}(\boldsymbol{V}_i^H\boldsymbol{V}_i).\end{aligned} \tag{18}$$

Since it is easy to find that $\operatorname{tr}(\boldsymbol{\Theta}_k\boldsymbol{\Theta}_k^H - \boldsymbol{\Theta}_i\boldsymbol{\Theta}_i^H) = 0$, (18) can be simplified into

$$\mathbb{E}\{\rho_i\} = -\operatorname{tr}(\boldsymbol{V}_i^H\boldsymbol{V}_i). \tag{19}$$

The variance of ρ_i is

$$\begin{aligned}\mathbb{V}\{\rho_i\} &= \mathbb{V}\{D_k\} + \mathbb{V}\{D_i\} + \operatorname{cov}\{D_k, D_i\}\\ &= L\sigma^4\operatorname{tr}(\boldsymbol{\Theta}_i\boldsymbol{\Theta}_i^H\boldsymbol{\Theta}_i\boldsymbol{\Theta}_i^H + \boldsymbol{\Theta}_k\boldsymbol{\Theta}_k^H\boldsymbol{\Theta}_k\boldsymbol{\Theta}_k^H)\\ &\quad + 2\sigma^2\operatorname{tr}(\boldsymbol{V}_i^H\boldsymbol{\Theta}_i^H\boldsymbol{\Theta}_i\boldsymbol{V}_i),\end{aligned} \tag{20}$$

where the covariance term $\operatorname{cov}\{D_k, D_i\}$ is ignored because D_k and D_i are weakly correlated. With simple manipulations, it proves that $\boldsymbol{\Theta}_k\boldsymbol{\Theta}_k^H\boldsymbol{\Theta}_k\boldsymbol{\Theta}_k^H = \boldsymbol{\Theta}_k\boldsymbol{\Theta}_k^H$ and $\boldsymbol{\Theta}_i\boldsymbol{\Theta}_i^H\boldsymbol{\Theta}_i\boldsymbol{\Theta}_i^H = \boldsymbol{\Theta}_i\boldsymbol{\Theta}_i^H$. Thus, (20) can be simplified into

$$\mathbb{V}\{\rho_i\} = L\sigma^4\operatorname{tr}(\boldsymbol{\Theta}_i\boldsymbol{\Theta}_i^H + \boldsymbol{\Theta}_k\boldsymbol{\Theta}_k^H) + 2\sigma^2\operatorname{tr}(\boldsymbol{V}_i^H\boldsymbol{V}_i). \tag{21}$$

Since ρ_i follows Gaussian distribution, the value of $\Pr(\rho_i \leq 0|\mathcal{H}_k)$ can be calculated by the pdf of ρ_i as

$$\Pr(\rho_i \leq 0|\mathcal{H}_k) = \int_{-\infty}^{0} f_{\rho_i}(t)\mathrm{d}t \quad = \frac{1}{2}\left(1+\operatorname{erf}\left(\tfrac{0-\mathbb{E}(\rho_i)}{\sqrt{2\mathbb{V}(\rho_i)}}\right)\right), \tag{22}$$

where $f_{\rho_i}(\cdot)$ denotes the pdf of ρ_i. Substituting (19) and (21) into (22), $\Pr(\rho_i \leq 0|\mathcal{H}_k)$ is rewritten as

$$\begin{aligned}&\Pr(\rho_i \leq 0|\mathcal{H}_k) =\\ &\frac{1}{2}\left(1+\operatorname{erf}\left(\frac{\operatorname{tr}(\boldsymbol{V}_i^H\boldsymbol{V}_i)}{\sqrt{2L\sigma^4\operatorname{tr}(\boldsymbol{\Theta}_i\boldsymbol{\Theta}_i^H+\boldsymbol{\Theta}_k\boldsymbol{\Theta}_k^H)+4\sigma^2\operatorname{tr}(\boldsymbol{V}_i^H\boldsymbol{V}_i)}}\right)\right).\end{aligned} \tag{23}$$

Substituting (4) and (23) into (13) leads to a tight expression of ζ_{MLE} as

$$\begin{aligned}&\zeta_{\mathrm{MLE}} = 1-\\ &\prod_{i,i\neq k}^{K}\frac{1}{2}\left(1+\operatorname{erf}\left(\frac{\operatorname{tr}(\boldsymbol{V}_i^H\boldsymbol{V}_i)}{\sqrt{2L\sigma^4\operatorname{tr}(\boldsymbol{\Theta}_i\boldsymbol{\Theta}_i^H+\boldsymbol{\Theta}_k\boldsymbol{\Theta}_k^H)+4\sigma^2\operatorname{tr}(\boldsymbol{V}_i^H\boldsymbol{V}_i)}}\right)\right).\end{aligned} \tag{24}$$

With the closed-form DER, we are able to conclude a series important insights, summarized in the remarks below.

Remark 2: For classic anonymity-agnostic precoders, their design utilities can be rate, user fairness, power minimization, or weighted signal-to-interference-and-noise ratio (SINR) maximization. Since the value of $\operatorname{tr}(\boldsymbol{V}_i^H\boldsymbol{V}_i)$ is typically a non-zero finite number, a small or moderate value of noise variance makes the value of the error function in (24) approach 1, meaning that the receiver can correctly reveal the real sender. By contrast, the anonymous precoder manipulates the signaling pattern to let the value of $\operatorname{tr}(\boldsymbol{V}_i^H\boldsymbol{V}_i)$ approach 0. As a result, user i acts as an alias sender, and makes the receiver unable to distinguish the real sender k and the alias i. Evidently, to achieve better DER performance, one needs to add more anonymous constraints, and let the associated value of $\operatorname{tr}(\boldsymbol{V}_i^H\boldsymbol{V}_i)$ approach 0.

Remark 3: As block length L increases, the value of the error function in (12) and (24) gradually approaches 1. As a result, DER of the MFN and MLE detectors gradually approaches 0. In other words, with more samples for sender detection, it becomes easier to identify the sender. Also, a small value of σ^2 makes the value of the error function in (12) and (24) approach 1, resulting in better DER performance of MFN and MLE detectors. Similar to the impact of noise, different forms of interference, such as the inter-cell interference, helps improve the anonymity.

Remark 4: As the MFN and MLE detectors exploit the users' CSI for sender detection, the DER performance is dependent of the channel correlation among users. As the correlation among user channels increases, the detection accuracy of the detectors gradually decreases. When there is a strong correlation between the channels of user k and i, the channel characteristics of $\boldsymbol{H}_k$ and $\boldsymbol{H}_i$ become similar, which makes $\mathrm{tr}(\boldsymbol{U}_k^H\boldsymbol{U}_k-\boldsymbol{U}_i^H\boldsymbol{U}_i)$ and $\mathrm{tr}(\boldsymbol{V}_i^H\boldsymbol{V}_i)$ approach 0. As a result, it becomes difficult for the BS to distinguish the real sender.

Remark 5: The MLE detector identifies the sender by exploiting the difference in distributions of D_k and D_i. As shown in subsection II-B2, D_i $(\forall i \neq k)$ involves the term $(\boldsymbol{H}_i\boldsymbol{H}_i^{\dagger}-\boldsymbol{I}_{N_r})\boldsymbol{H}_k\boldsymbol{W}_k\boldsymbol{S}_k$ and colored noise, while D_k only contains a colored noise. However, for the MFN detector, both G_k and G_i contain the signal related term and colored noise, as shown in subsection II-B1. As a result, the detection accuracy of MFN detector is inferior to that of the MLE detector, but is with lower computational complexity.

IV. Simulation Results

To verify the tightness of the analytic results, Monte Carlo simulation is carried out. Quadrature phase shift keying is used in modulation. Assume that there are $K = 5$ users, and the signal sender is randomly generated per slot. The energy detection threshold is $\varepsilon = 10^{-2}$, and the antenna configuration of the BS and the user is $N_r = 9$ and $N_t = 8$ respectively. We normalize the maximum power $p_{\max} = 1$ watt, while changing SNR by tuning the noise power. Assume that the block size $L = 50$. Consider Rayleigh block fading MIMO channel, we evaluate the following classic precoders: 1) MMSE precoder [9], 2) SVD precoder [10], 3) PM precoder [11], 4) constructive interference (CI) precoder [15], 5) CI-based anonymous (CIA) precoder [5]. Note that CI and CIA precoders perform at symbol-by-symbol level, while others perform at block-by-block level. Also, the CIA precoder is specifically designed for anonymity, which manipulates the transmitted signal for masking the real sender.

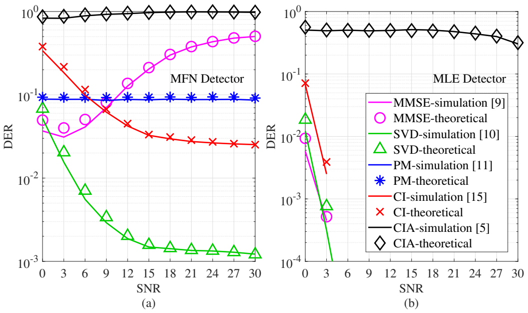

Fig. 2. The impact of transmit-SNR on the DER by different precoders. $N_t = 8$, $N_r = 9$. The per-antenna SINR of the PM precoder is set to 5 dB. The anonymous related thresholds of CIA (against MFN) and CIA (against MLE) precoders are set to 2 and 0.01.

To evaluate the deviation between the closed-form and actual DER results, the NMSE is defined as $\mathrm{NMSE} = \frac{\sum_{m=1}^{M}(\mathrm{DER}_c^m-\mathrm{DER}_a^m)^2}{\sum_{m=1}^{M}(\mathrm{DER}_a^m)^2}$, where DER_a^m and DER_c^m denote the actual and derived closed-form DER results in the m-th simulation, and M denotes the total number of the simulation results. Fig. 2 shows the closed-form and actual DER results of the MFN and MLE detectors. It is observed that the closed-form DER is close to the actual DER regardless of the employed precoders and SNR statuses. Typically, with a generic precoder, the NMSE between the closed-form and actual DER results is on the levels of $0 \sim 10^{-1}$ for the MFN and MLE detectors. It is observed that a high level of SNR improves the detection performance of the MFN detector. However, when the MMSE precoder is applied by the user, the DER of the MFN detector increases with the increase of the SNR. It is because the structure of the MMSE precoder approaches that of the ZF precoder with a small value of noise, which removes the sender's CSI from the received signal. As a result, the MMSE precoder occasionally achieves better anonymity at high SNR regime. Also, it proves that the CIA precoder obtains a higher DER and hence a better anonymity performance than other anonymity-agnostic precoders. It validates our analysis in Remarks 1 and 2 that, by manipulating transmitted signaling pattern, the DER performance of sender detection can be scrambled. Note that the DER of the PM precoder is not visible in Fig. 2 (b), as the DER of the MLE detector by the PM precoder is reduced to 0. Also, although the MMSE precoder approaches the ZF precoder at high SNR regime, the MLE detector still identifies the sender. It is because D_k and D_i can be distinguished due to their different statistics, as analyzed in subsection II-B2. In addition, it shows that the MLE detector achieves better detection accuracy then the MFN detector, validating the analysis in Remark 5.

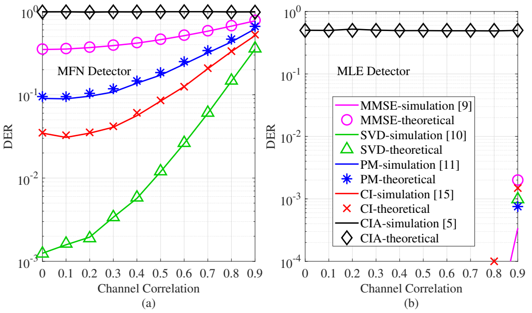

Fig. 3. The impact of channel correlation on the DER by different precoders. $N_t = 8$, $N_r = 9$. The per-antenna SINR of the PM precoder is set to 5 dB. The anonymous related thresholds of CIA (against MFN) and CIA (against MLE) precoders are set to 2 and 0.01, while the transmit-SNR is set to 20 dB and 10 dB.

Fig. 3 shows the closed-form and actual DER results with different channel correlation coefficients. Based on the Pearson correlation coefficient [16], the channel correlation coefficient between MIMO channel matrices $\boldsymbol{H}_i$ and $\boldsymbol{H}_j$ is defined as $\omega_{ij} = \frac{\sum_{m=1}^{N_r}\sum_{n=1}^{N_t}([\boldsymbol{H}_i]_{mn}-\bar{\boldsymbol{H}}_i)([\boldsymbol{H}_j]_{mn}-\bar{\boldsymbol{H}}_j)}{\sqrt{\left(\sum_{m=1}^{N_r}\sum_{n=1}^{N_t}([\boldsymbol{H}_i]_{mn}-\bar{\boldsymbol{H}}_i)^2\right)\left(\sum_{m=1}^{N_r}\sum_{n=1}^{N_t}([\boldsymbol{H}_j]_{mn}-\bar{\boldsymbol{H}}_j)^2\right)}}$, where $\bar{\boldsymbol{H}}_i = \frac{1}{N_rN_t}\sum_{m=1}^{N_r}\sum_{n=1}^{N_t}[\boldsymbol{H}_i]_{mn}$ and $\bar{\boldsymbol{H}}_j = \frac{1}{N_rN_t}\sum_{m=1}^{N_r}\sum_{n=1}^{N_t}[\boldsymbol{H}_j]_{mn}$, $i \neq j$. It is observed that the closed-form DER is close to the actual DER regardless of the employed precoders and the correlation coefficient. The NMSE between the closed-form and actual DER results is on the levels of $10^{-3} \sim 10^{-2}$ for the MFN and MLE detectors. With the increase of channel correlation, the DER by the

CIA precoder is maintained at a high level, while DER by other anonymity-agnostic precoders shows an upward trend. In particular, the DER by the anonymity-agnostic precoders in Fig. 3 (b) reduces to 0 when channel correlation coefficient is less than 0.8, which is thus not visible.

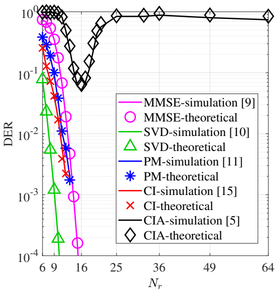

Fig. 4. The impact of different antenna configurations on the DER of the MFN detector by different precoders, where N_t=8. The per-antenna SINR of the PM precoder is set to 5 dB. The anonymous related thresholds of the CIA precoder is set to 2. The transmit-SNR is set to 20 dB.

Fig. 4 shows the closed-form and actual DER results of the MFN detector with different numbers of receive-antennas. It is observed that the closed-form DER is close to the actual DER. Typically, with a generic precoder, the NMSE between the closed-form and actual DER results is on the levels of $0 \sim 10^{-2}$. When the classic MMSE, SVD, PM, CI precoders are employed by the users, DER of the MFN detector decreases with the increase of N_r. It is because a large number of N_r means there are more samples for detection, resulting in better DER performance. Also, when N_r is less than 16, DER by the CIA precoder decreases with the increase of N_r. It is because with a fixed anonymity threshold, the anonymous constraint of the CIA precoder becomes stricter when the dimension of the channel matrix increases. However, when $N_r > 16$, the DER by the CIA precoder shows an upward trend. It is because the CIA always tries to multiplex N_r streams under the anonymous constraint. As a result, the CIA precoder tends to use lower power which occasionally helps the anonymity performance at the cost of low communication performance. Due to page limit, the impact of N_r on the DER performance by the MLE detector is not demonstrated.

V. Conclusion

In this paper, the DER performance of two classic PHY sender detectors has been theoretically analyzed, and their tight closed-form expressions have been derived. Based on the analytic DER results, we have theoretically built the relation between the instantaneous signaling pattern and the statistical DER performance for generic precoders. In addition, a series of important insights have been presented, such as the impact of block length, noise status, and precoder on the DER performance. Finally, we have benchmarked the derived closed-form DER against actual results, and the tightness of the derived closed-form results has been verified.

Appendix
Proof of Lemma 1

Denote $\boldsymbol{y}_{(j)}$, $\boldsymbol{u}_{i(j)}$ and $\boldsymbol{\mu}_{(j)}$ as the j-th column of $\boldsymbol{Y}$, $\boldsymbol{U}_i$ and $\boldsymbol{H}_k\boldsymbol{W}_k\boldsymbol{S}_k$, respectively. We have that $G_i = \sum_{j=1}^{L} \|\boldsymbol{H}_i^H\boldsymbol{y}_{(j)}\|_2^2$, where $\boldsymbol{y}_{(j)} \sim \mathcal{N}(\boldsymbol{\mu}_{(j)}, \boldsymbol{\Lambda})$ and $\boldsymbol{\Lambda} = \sigma^2\boldsymbol{I}_{N_r}$. Since the term $\|\boldsymbol{H}_i^H\boldsymbol{y}_{(j)}\|_2^2$ is quadratic with respect to $\boldsymbol{y}_{(j)}$, its expectation is calculated as

$$\mathbb{E}\{\|\boldsymbol{H}_i^H\boldsymbol{y}_{(j)}\|_2^2\} = \sigma^2\mathrm{tr}(\boldsymbol{H}_i\boldsymbol{H}_i^H) + \boldsymbol{u}_{i(j)}^H\boldsymbol{u}_{i(j)}. \tag{25}$$

Let $\boldsymbol{D}(t) = \boldsymbol{I}_{N_r} - 2t\boldsymbol{H}_i\boldsymbol{H}_i^H\boldsymbol{\Lambda}$, and the moment generating function of $\boldsymbol{y}_{(j)}^H\boldsymbol{H}_i\boldsymbol{H}_i^H\boldsymbol{y}_{(j)}$ is written as $M(t)=|\boldsymbol{D}|^{-\frac{1}{2}}e^{-\frac{1}{2}[\boldsymbol{I}_{N_r}-\boldsymbol{D}^{-1}(t)]\boldsymbol{\Lambda}^{-1}\boldsymbol{\mu}_{(j)}}$. We further let $k(t) = \ln(M(t))$, and denote its second-order derivative as $k''(t)$. Substituting the value of $|\boldsymbol{D}|_{t=0}$, $\frac{\mathrm{d}|\boldsymbol{D}|}{\mathrm{d}t}|_{t=0}$, $\frac{\mathrm{d}^2|\boldsymbol{D}|}{\mathrm{d}t^2}|_{t=0}$, $\boldsymbol{D}|_{t=0}$, $\boldsymbol{D}^{-1}|_{t=0}$, $\frac{\mathrm{d}\boldsymbol{D}}{\mathrm{d}t}|_{t=0}$ and $\frac{\mathrm{d}^2\boldsymbol{D}}{\mathrm{d}t^2}|_{t=0}$ into $k''(t)$, we have

$$\mathbb{V}\{\|\boldsymbol{H}_i^H\boldsymbol{y}_{(j)}\|_2^2\} = \sigma^4\mathrm{tr}(\boldsymbol{H}_i\boldsymbol{H}_i^H\boldsymbol{H}_i\boldsymbol{H}_i^H) + 2\sigma^2\boldsymbol{u}_{i(j)}^H\boldsymbol{H}_i^H\boldsymbol{H}_i\boldsymbol{u}_{i(j)}. \tag{26}$$

Considering the block length L, the expectation and variance of G_i are

$$\mathbb{E}\{G_i\} = L\sigma^2\mathrm{tr}(\boldsymbol{H}_i\boldsymbol{H}_i^H) + \mathrm{tr}(\boldsymbol{U}_i^H\boldsymbol{U}_i), \tag{27}$$

and

$$\mathbb{V}\{G_i\} = L\sigma^4\mathrm{tr}(\boldsymbol{H}_i\boldsymbol{H}_i^H\boldsymbol{H}_i\boldsymbol{H}_i^H) + 2\sigma^2\mathrm{tr}(\boldsymbol{U}_i^H\boldsymbol{H}_i^H\boldsymbol{H}_i\boldsymbol{U}_i). \tag{28}$$

References

[1] J. Wang *et al.*, "Blockchain-based anonymous authentication with key management for smart grid edge computing infrastructure," *IEEE Trans. Industr. Inform.*, vol. 16, no. 3, pp. 1984–1992, 2020.

[2] S. Tangade, S. S. Manvi, and P. Lorenz, "Trust management scheme based on hybrid cryptography for secure communications in vanets," *IEEE Trans. Veh. Technol.*, vol. 69, no. 5, pp. 5232–5243, 2020.

[3] R. Soltani, D. Goeckel, D. Towsley, B. A. Bash, and S. Guha, "Covert wireless communication with artificial noise generation," *IEEE Trans. Wireless Commun.*, vol. 17, no. 11, pp. 7252–7267, 2018.

[4] Y. Yang *et al.*, "A survey on security and privacy issues in internet-of-things," *IEEE Internet Things J.*, vol. 4, no. 5, pp. 1250–1258, 2017.

[5] Z. Wei *et al.*, "Fundamentals of physical layer anonymous communications: Sender detection and anonymous precoding," *IEEE Trans. Wireless Commun.*, vol. 21, no. 1, pp. 64–79, 2022.

[6] J. Shen, T. Zhou, X. Chen, J. Li, and W. Susilo, "Anonymous and traceable group data sharing in cloud computing," *IEEE Trans. Inf. Forensics Security*, vol. 13, no. 4, pp. 912–925, 2018.

[7] J. Liu, Z. Zhang, X. Chen, and K. S. Kwak, "Certificateless remote anonymous authentication schemes for wirelessbody area networks," *IEEE Trans. Parallel Distrib. Syst.*, vol. 25, no. 2, pp. 332–342, 2013.

[8] M. Sayad Haghighi and Z. Aziminejad, "Highly anonymous mobility-tolerant location-based onion routing for vanets," *IEEE Internet Things J.*, vol. 7, no. 4, pp. 2582–2590, 2020.

[9] A. Wiesel *et al.*, "Zero-forcing precoding and generalized inverses," *IEEE Trans. Signal Process.*, vol. 56, no. 9, pp. 4409–4418, 2008.

[10] F. Sohrabi and W. Yu, "Hybrid digital and analog beamforming design for large-scale antenna arrays," *IEEE J. Sel. Top. Signal Process.*, vol. 10, no. 3, pp. 501–513, 2016.

[11] R. López-Valcarce and N. González-Prelcic, "Hybrid beamforming designs for frequency-selective mmwave mimo systems with per-rf chain or per-antenna power constraints," *IEEE Trans. Wireless Commun.*, vol. 21, no. 8, pp. 5770–5784, 2022.

[12] Z. Wei *et al.*, "Physical layer anonymous precoding design: From the perspective of anonymity entropy," *IEEE J. Sel. Areas Commun.*, vol. 40, no. 11, pp. 3224–3238, 2022.

[13] E. Axell, G. Leus, E. G. Larsson, and H. V. Poor, "Spectrum sensing for cognitive radio : State-of-the-art and recent advances," *IEEE Trans. Signal Process.*, vol. 29, no. 3, pp. 101–116, 2012.

[14] T. Y. Al-Naffouri *et al.*, "On the distribution of indefinite quadratic forms in gaussian random variables," *IEEE Trans. Commun.*, vol. 64, no. 1, pp. 153–165, 2016.

[15] C. Masouros and G. Zheng, "Exploiting known interference as green signal power for downlink beamforming optimization," *IEEE Trans. Signal Process.*, vol. 63, no. 14, pp. 3628–3640, 2015.

[16] I. Cohen *et al.*, "Pearson correlation coefficient," *Noise reduction in speech processing*, pp. 1–4, 2009.